materials

MDPI

Article

High-Pressure Structures and Superconductivity of Barium Iodide

Shubo Wei [1,2] and Hanyu Liu [1,2,*]

[1] State Key Laboratory for Superhard Materials, College of Physics, Jilin University, Changchun 130012, China; weishubo.good@163.com
[2] International Center for Computational Methods and Software, College of Physics, Jilin University, Changchun 130012, China
* Correspondence: hanyuliu@jlu.edu.cn

Abstract: Generally, pressure is a useful tool to modify the behavior of physical properties of materials due to the change in distance between atoms or molecules in the lattice. Barium iodide (BaI_2), as one of the simplest and most prototypical iodine compounds, has substantial high pressure investigation value. In this work, we explored the crystal structures of BaI_2 at a wide pressure range of 0–200 GPa using a global structure search methodology. A thermodynamical structure with tetragonal $I4/mmm$ symmetry of BaI_2 was predicted to be stable at 17.1 GPa. Further electronic calculations indicated that $I4/mmm$ BaI_2 exhibits the metallic feature via an indirect band gap closure under moderate pressure. We also found that the superconductivity of BaI_2 at 30 GPa is much lower than that of CsI at 180 GPa based on our electron–phonon coupling simulations. Our current simulations provide a step toward the further understanding of the high-pressure behavior of iodine compounds at extreme conditions.

Keywords: high pressure; superconductivity; crystal structure prediction; phase transition

Citation: Wei, S.; Liu, H. High-Pressure Structures and Superconductivity of Barium Iodide. *Materials* **2022**, *15*, 522. https://doi.org/10.3390/ma15020522

Academic Editor: Alexandros Lappas

Received: 7 December 2021
Accepted: 5 January 2022
Published: 10 January 2022

1. Introduction

A large number of interesting properties of iodine compounds have been reported such as optical properties, conduction characteristics, catalytic performance, medical application and the hypervalence phenomenon [1–10]. Barium iodide (BaI_2), as one of the simplest and most representative ionic iodine compounds, has attracted plentiful studies [11–15]. At ambient pressure, barium iodide (BaI_2) shares a cotunnite-type structure (orthorhombic $Pnma$, $Z = 4$) [11] with many other dihalides AX_2 (A = Ca, Ba, Pb, Sn) [16] Under high pressure, a new high-pressure phase of BaI_2 with monoclinic $P112_1/a$ ($Z = 8$) symmetry between 12 and 15 GPa was reported in 1995 [13]. Curiously, this previous work identified the monoclinic $P112_1/a$ phase at a pressure range of 20–40 GPa [13]. Moreover, the latest theoretical work in 2015 reported that BaI_2 maintains insulator characteristics at least up to 40 GPa [15]. The superconducting behavior of CsI has been reported by experimental and theoretical works [7,17,18], where the external pressure reached 180 GPa. BaI_2, as one of the most representative iodine compounds, shares a similar prototype with CsI. According to the reported superconducting mechanism of CsI, the increasing number of electrons of Cs is responsible for superconductivity, and the Ba atom with more electrons is potentially superior to the Cs atom in the electron–phonon coupling. Thus, it is an interesting topic to investigate the conduction characteristics at lowering pressure, which implies much more application value. To the best of our knowledge, the highest pressure studied in previous work for BaI_2 was lower than 40 GPa, and the whole high-pressure structural transition sequence up to 200 GPa is still far from being clear and well established. These structural uncertainties impede the in-depth understanding and further exploration of the electronic properties of BaI_2 under compression.

Here, we present systematic structure searches for BaI_2 at high pressures using our developed CALYPSO method [19–22]. Our results show that BaI_2 adopts orthorhombic

Pnma symmetry at 0 GPa, which is consistent with experimental work [11,13]. Furthermore, we identified one thermodynamically stable tetragonal $I4/mmm$ phase for BaI_2 at high pressure which is energetically superior to the previously reported post-cotunnite phase ($P112_1/a$, $Z = 8$) [13]. Further electronic calculations showed that BaI_2 becomes a metallic phase via indirect band gap closure at moderate compression. In addition, the simulations also suggest the superconductive feature of BaI_2 at 30 GPa [7].

2. Computational Details

To obtain stable high-pressure structures of BaI_2, we carried out a global structure search by our developed CALYPSO (Crystal structure AnaLYsis by Particle Swarm Optimization) method [19–22] within the first-principle electronic structure. This computational scheme was verified by many works [23–27]. We used Perdew–Burke–Ernzerhof generalized gradient approximation (PBE-GGA) [28] exchange correlation for the simulations, where the VASP (Vienna ab initio simulation package) code was also employed [29]. Furthermore, we used the Phonopy code to investigate the dynamic properties of the predicted structures [30]. The Device Studio [31] program provides a number of functions for performing visualization, modeling and simulation. We used Bader's quantum theory of atoms in molecules (QTAIM) analysis [32] to investigate the charge properties of the predicted structures. Superconductivity was studied by density-functional perturbation theory [33,34], where the Quantum-ESPRESSO package [35,36] was used.

3. Results and Discussion

To uncover stable structures of BaI_2, we performed systematic structural predictions at a pressure range of 0–200 GPa without considering temperature effects, with the CALYPSO methodology [19–22]. According to our simulations, at ambient pressure, the cotunnite-type *Pnma* ($Z = 4$) phase of BaI_2 is the thermodynamically optimal structure (Figure 1). From Figure 1c, each barium atom was surrounded by nine iodine atoms, and all the atoms of the primitive cell were packed in an orthorhombic cage. The optimized lattice parameter of the *Pnma* phase takes $a = 9.003$ Å, $b = 5.448$ Å and $c = 10.879$ Å at ambient pressure, which is close to experiment data with $a = 8.922$ Å, $b = 5.304$ Å and $c = 10.695$ Å [11]. The agreement between our current simulations and experimental studies [11,13,15] provides a validation of the present simulation scheme.

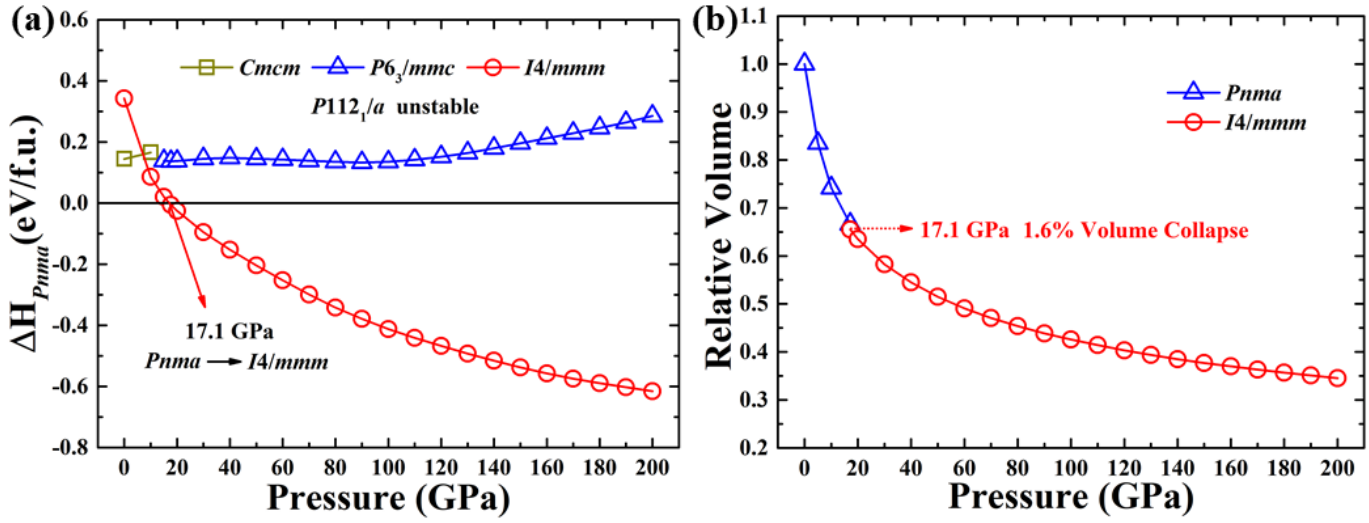

Figure 1. *Cont.*

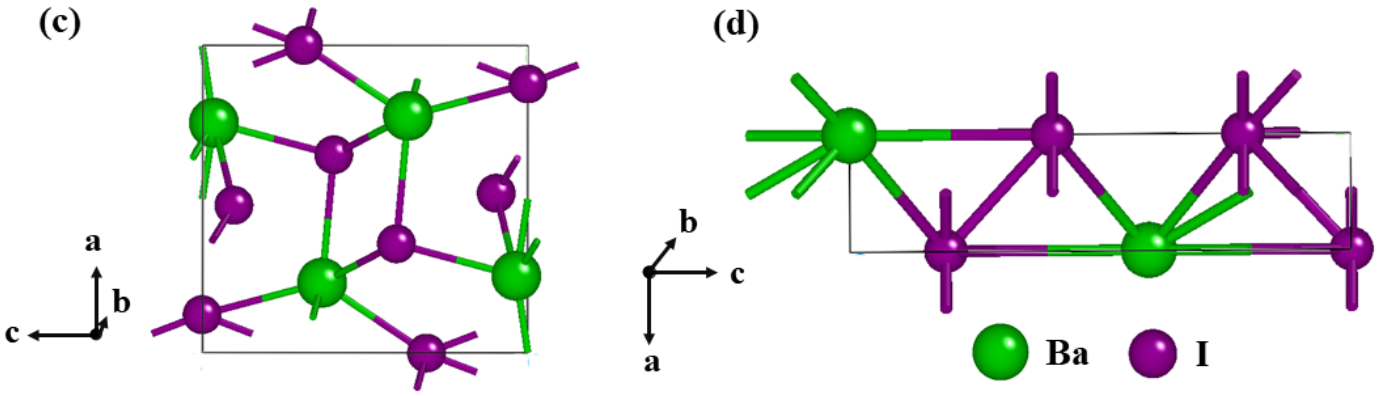

Figure 1. (**a**) Enthalpies (related to the *Pnma* phase) of *Cmcm*, $P6_3/mmc$ and $I4/mmm$ structures of BaI_2. The former reported $P112_1/a$ structure[13] is thermodynamically unstable. (**b**) The relative volume of BaI_2. The crystal structure of orthorhombic *Pnma* (**c**) and tetragonal $I4/mmm$ (**d**) of $BaCl_2$ at 0.3 and 17.1 GPa, respectively.

Under high pressure, we found the stability of the *Pnma* structure at a pressure range of 0–17 GPa, after which it undergoes a phase transition into the tetragonal $I4/mmm$ phase ($Z = 2$), with nearly no volume collapse, as shown in Figure 1. Comparing with the *Pnma* structure, the $I4/mmm$ phase has a higher symmetry with a coordination of 10. We provide the lattice parameters and atomic coordinates in Table 1. Earlier experimental work showed the existence of a monoclinic $P112_1/a$ phase of BaI_2 at a pressure range of 12–15 GPa at room temperature.[13] According to the lattice parameters and atomic positions in the current work, we calculated the enthalpy of the experimentally known monoclinic $P112_1/a$ structure, and our results indicate that this $P112_1/a$ structure has a higher enthalpy than our predicted structure. The enthalpy curve of $P112_1/a$ is not shown due to its large number compared with the reference enthalpy lines. The $P6_3/mmc$ and *Cmcm* phases, as underlying stable structures obtained during the structure prediction process, were also taken into account in the comparison (Figure 1a). We also provide the X-ray diffraction patterns of these structures in Figure 2, and the future experiment is thus stimulated. Our work shows that BaI_2 follows the following structural progression: orthorhombic *Pnma* (0–17.1 GPa) → tetragonal $I4/mmm$ (17.1–200 GPa). Our simulations also suggest the dynamical stability feature of the predicted structures, as shown in Figure 2.

Table 1. Lattice parameters and atomic coordinates of BaI_2.

Phase	Lattice Parameters (Å)	Atoms	*x*	*y*	*z*
Pnma BaI_2	$a = 9.003$	Ba1 (4c)	0.24	0.75	0.61
0.001 GPa	$b = 5.448$	I1 (4c)	0.64	0.75	0.58
	$c = 10.879$	I2 (4c)	0.48	0.25	0.84
$I4/mmm$ BaI_2	$a = 4.094$	Ba (2a)	0.00	0.00	0.00
17.1 GPa	$b = 4.094$	I (4e)	0.50	0.50	0.16
	$c = 10.434$				
$I4/mmm$ BaI_2	$a = 3.255$	Ba (2a)	0.00	0.00	0.00
200 GPa	$b = 3.255$	I (4e)	0.50	0.50	0.17
	$c = 8.695$				

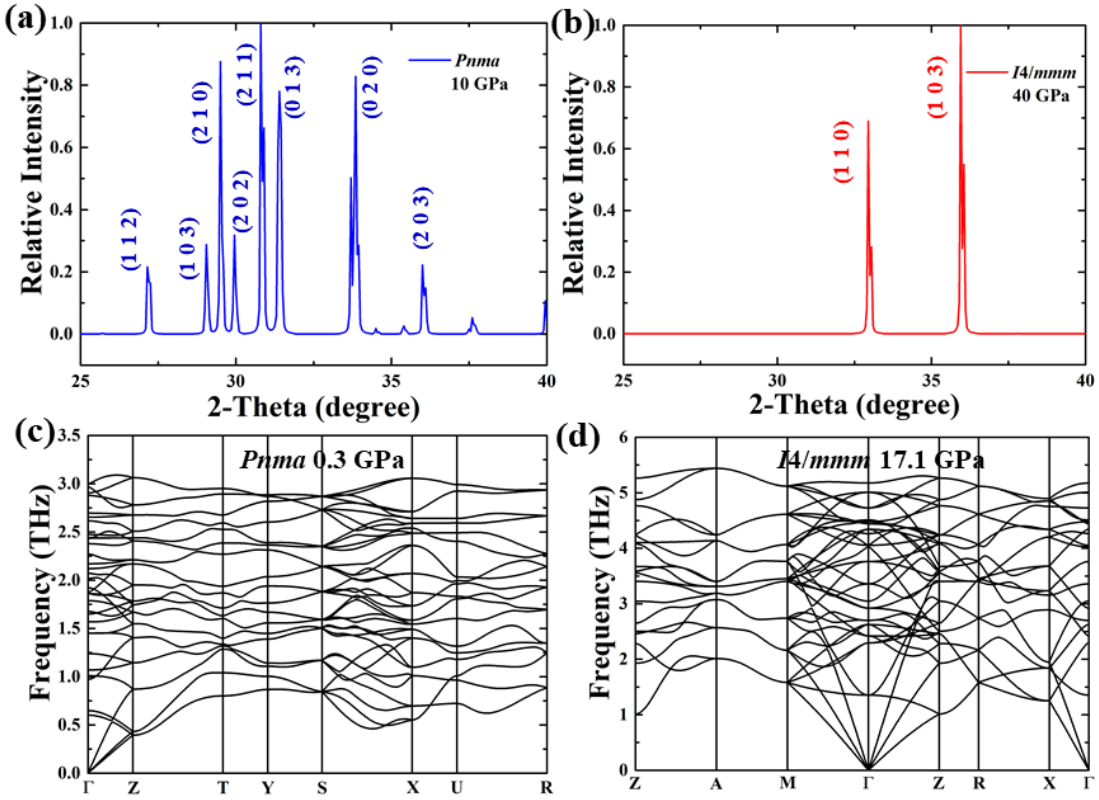

Figure 2. The simulated power X-ray diffraction, where λ of 1.54 Å was used for *Pnma* BaI_2 at 10 GPa (**a**) and *I*4/*mmm* BaI_2 at 40 GPa (**b**). Calculated phonon spectra of *Pnma* BaI_2 at 0.3 GPa (**c**) and *I*4/*mmm* BaI_2 at 75 GPa (**d**).

In this work, we also provide the Bader charge and the Ba–I bond distance in Figure 3. These simulations suggest the peculiar reverse of the charge transfer between Ba and I atoms.

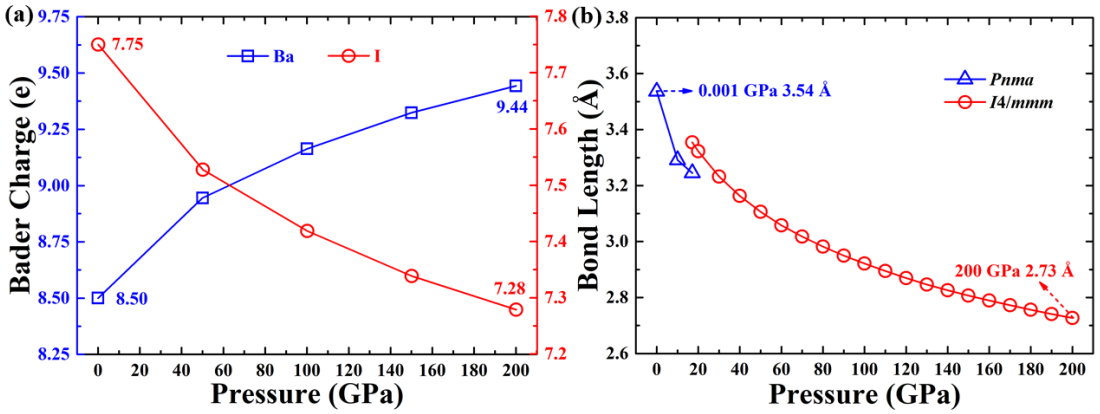

Figure 3. (**a**) Simulated Bader charge for BaI_2. (**b**) The distance between B and I atoms.

Previous studies suggested that CsCl, CsBr and CsI are metallic phases at high pressures [7,37]. At ambient conditions, BaI_2 has a wide band gap between valance and conductive bands, with a value of 3.51 eV (Figure 4a). Interestingly, our studies also show the metallic feature of BaI_2 at a moderate pressure of 30 GPa (Figure 4), which is quite different from the direct band gap closure in the CsCl and CsBr systems [37]. The latest theoretical work in 2015 reported that BaI_2 maintains its insulating feature up to 40 GPa [15]. It is noteworthy that it adopts the ambient orthorhombic *Pnma* structure, which is obviously not accurate without considering high-pressure phases. Therefore, the newly

predicted tetragonal phase with *I*4/*mmm* symmetry is responsible for this pressure-induced metallization.

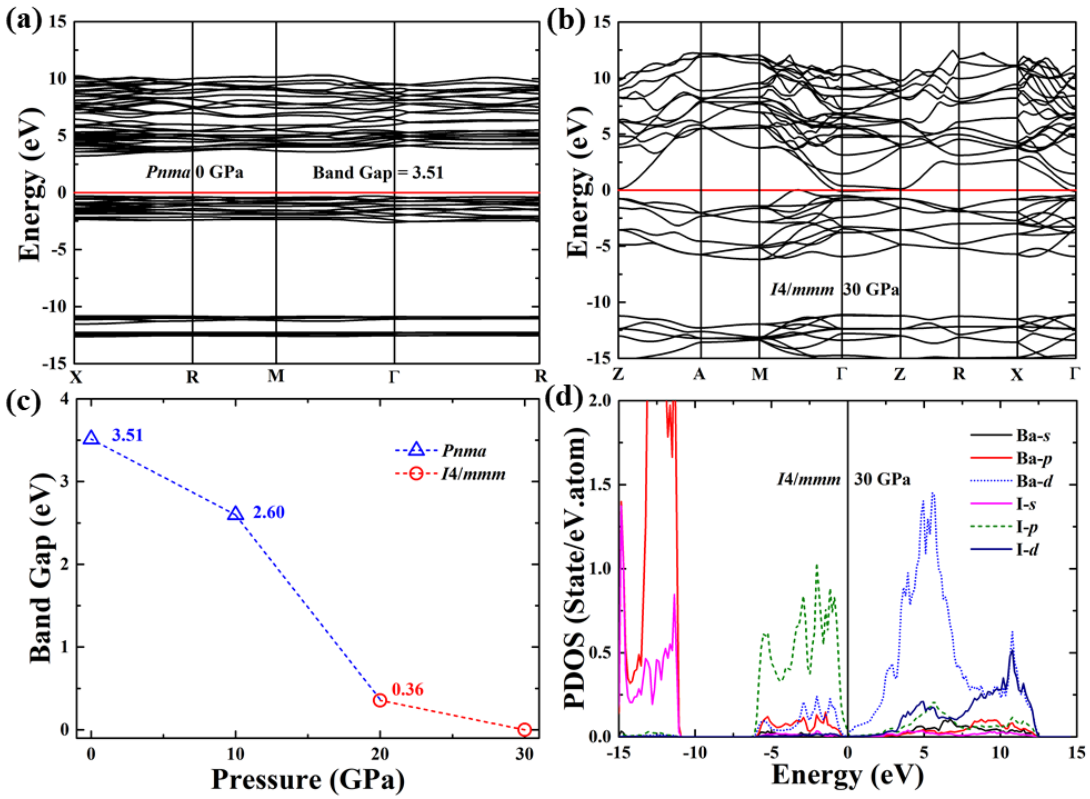

Figure 4. Calculated electronic band plot along high-symmetry directions of *Pnma* BaI_2 at 0 GPa (**a**) and *I*4/*mmm* BaI_2 at 30 GPa (**b**). Pressure dependence of theoretical band gaps of BaI_2 (**c**). Electronic density of states of *I*4/*mmm* BaI_2 at 30 GPa (**d**).

The superconducting behavior of CsI has been extensively explored by experimental and theoretical methods [7,17–19]. Therefore, it is noteworthy to study the superconductivity of BaI_2 at high pressure. In this work, we performed electron–phonon coupling calculations for BaI_2. We provide the Eliashberg spectral function $\alpha^2F(\omega)$ [38] (Figure 5) and the phonon density of states (PHDOS) of BaI_2 at 30 GPa. It is clearly seen that $\alpha^2F(\omega)$ can be roughly divided into three parts: low (0.49–1.25 THz), medium (1.25–5.78 THz) and high frequency (5.78–6.51 THz). We employed the Allen–Dynes modified McMillan equation [39] $T_c = \frac{\omega_{\log}}{1.2} \exp\left[-\frac{1.04(1+\lambda)}{\lambda-\mu^*(1+0.62\lambda)}\right]$ to estimate the superconductivity of the predicted structures, where $\omega_{\log}$ is the logarithmic average frequency, and μ^* is the Coulomb pseudopotential. At 30 GPa, $\omega_{\log}$ was 132.62 K, while at 200 GPa, it was 207.23 K. Furthermore, we found that the estimated superconducting critical temperature T_C for BaI_2 was 1.27 K at 30 GPa and 0.35 K at 200 GPa. Moreover, two recent studies reported non-adiabatic superconductivity in sibling BKBO [40] and low-dimensional LiC_6 [41]. These studies presented a coherent interpretation of the superconductivity. In our work, the relatively lower bottom of the conduction band of BaI_2 implies the potential influence of non-adiabatic effects, and this may be an interesting orientation in future work.

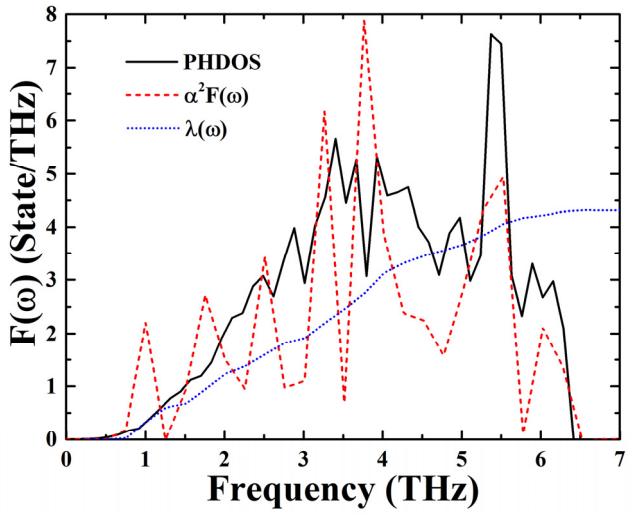

Figure 5. The electron–phonon coupling calculations of *I*4/*mmm* BaI_2 at 30 GPa.

4. Conclusions

We investigated the high-pressure crystal structures and electronic properties of BaI_2 up to 200 GPa. Our results suggest a thermodynamically stable tetragonal *I*4/*mmm* symmetry of BaI_2 identified at 17.1 GPa. The systematic increase in the coordination number from 9 to 10 should be seen in many AX_2 compounds. Furthermore, we uncovered that *I*4/*mmm* BaI_2 becomes a metallic phase at moderate pressure, which is different to *Pbam* CsCl and *Pmma* CsBr (via direct band gap closure at the Γ point) [37]. Our simulations suggest the superconducting feature of the predicted structure for BaI_2 at 30 GPa. Comparing with CsI, cesium xenide and barium xenide have a similar composition with more electrons, making them good subjects for study, with great potential to exhibit superconductivity at moderate pressure. Our work clarifies the high-pressure phase transition sequence of BaI_2 up to 200 GPa, which represents a step toward the understanding of the behavior of AX_2-type iodine compounds under extreme conditions.

Author Contributions: Conceptualization, S.W. and H.L.; Writing-original draft preparation, S.W.; Investigation, S.W. and H.L. All authors have read and agreed to the published version of the manuscript.

Funding: This work was supported by the National Natural Science Foundation of China (Grant Nos. 12074138, 11874175, 11874176), Fundamental Research Funds for the Central Universities and the Program for JLU Science and Technology Innovative Research Team (JLUSTIRT).

Institutional Review Board Statement: Not applicable.

Informed Consent Statement: Not applicable.

Data Availability Statement: The data presented in this study are available on request from the corresponding author.

Acknowledgments: S.W. and H.L. acknowledge the Facility of High-Performance Computing Center of Jilin University.

Conflicts of Interest: The authors declare no conflict of interest.

References

1. Philip, H.Y.; Charles, J.D. Some optical properties of potassium iodide-thallium phosphors. *J. Chem. Phys.* **1953**, *21*, 892–898.
2. Bradley, J.N.; Greene, P.D. Potassium iodide +silver iodide phase diagram high ionic conductivity of KAg4I5. *Trans. Faraday Soc.* **1966**, *62*, 2069–2075. [CrossRef]
3. Liang, C.C. Conduction characteristics of the lithium iodide-aluminum oxide solid electrolytes. *J. Electrochem. Soc.* **1973**, *120*, 1289. [CrossRef]
4. Dipak, P.; Jagir, S.S. Cadmium iodide as a new catalyst for knoevenagel condensations. *J. Chem. Soc. Perkin Trans.* **1993**, *1*, 739–740.

5. Smanik, P.A.; Liu, Q.; Furminger, T.L.; Ryu, K.; Xing, S.; Mazzaferri, E.L.; Jhiang, S.M. Cloning of the human sodium lodide symporter. *Biophys. Res. Commun.* **1996**, *226*, 339–345. [CrossRef]
6. Xie, W.; Li, H. Alumina-supported potassium iodide as a heterogeneous catalyst for biodiesel production from soybean oil. *J. Mol. Catal. A Chem.* **2006**, *255*, 1–9. [CrossRef]
7. Xu, Y.; John, S.T.; Artem, R.O.; Cui, T.; Wang, H.; Ma, Y.; Zou, G. Superconducting high-pressure phase of cesium iodide. *Phys. Rev. B* **2009**, *79*, 144110. [CrossRef]
8. Zhang, F.; Gale, J.D.; Uberuaga, B.P.; Stanek, C.R.; Marks, N.A. Importance of dispersion in density functional calculations of cesium chloride and its related halides. *Phys. Rev. B* **2013**, *88*, 054112. [CrossRef]
9. Wei, S.; Wang, J.; Deng, S.; Zhang, S.; Li, Q. Hypervalent iodine with linear chain at high pressure. *Sci. Rep.* **2015**, *5*, 14393. [CrossRef]
10. Li, Z.; Li, Q.; Li, H.; Yue, L.; Zhao, D.; Tian, F.; Dong, Q.; Zhang, X.; Jin, X.; Zhang, L.; et al. Pressure-tailored band engineering for significant enhancements in the photoelectric performance of CsI_3 in the optical communication waveband. *Adv. Funct. Mater.* **2021**, 2108636. [CrossRef]
11. Elizabeth, B.B.; Thomas, E.B.; Ronald, L.S. The crystal structures of barium chloride, barium bromide, and barium iodide. *J. Phys. Chem.* **1963**, *67*, 2132–2135.
12. Winchell, P. Mass spectrometric investigation of barium iodide and caesium iodide vaporizations. *Nature* **1965**, *206*, 1252. [CrossRef]
13. Leger, J.M.; Haines, J.; Atouf, A. The post-cotunnite phase in $BaCl_2$, $BaBr_2$ and BaI_2 under high pressure. *J. Appl. Cryst.* **1995**, *28*, 416. [CrossRef]
14. Nerine, J.C.; Giulia, H.; Alexander, D.D.; Stephen, A.P.; Edgar, L.; Cody, M.W.; Shah, K.S.; Utpal, N.R.; Arnold, B.; Lynn, A.; et al. Strontium and barium iodide high light yield scintillators. *Appl. Phys. Lett.* **2008**, *92*, 083508.
15. Pradeep, K.; Agnikumar, G.V. Pressure dependence of electronic properties of BaI_2. *AIP Conf. Proc.* **2015**, *1675*, 020013.
16. Raman, A.; Steinfink, H. Crystal chemistry of AB_2 structures. *Inorg. Chem.* **1967**, *6*, 1789. [CrossRef]
17. Eremets, M.I.; Shimizu, K.T.; Kobayashi, T.C.; Amaya, K. Metallic CsI at pressures of up to 220 gigapascals. *Science* **1998**, *281*, 1333. [CrossRef] [PubMed]
18. Eremets, M.I.; Shimizu, K.; Kobayashi, T.C.; Amaya, K. Metallization and superconductivity in CsI at pressures up to 220 GPa. *J. Phys. Condens. Matter* **1998**, *10*, 11519. [CrossRef]
19. Wang, Y.; Lv, J.; Zhu, L.; Ma, Y. CALYPSO: A method for crystal structure prediction. *Comput. Phys. Commun.* **2012**, *183*, 2063–2070. [CrossRef]
20. Wang, Y.; Lv, J.; Zhu, L.; Ma, Y. Crystal structure prediction via particle-swarm optimization. *Phys. Rev. B Condens. Matter Mater. Phys.* **2010**, *82*, 094116. [CrossRef]
21. Wang, Y.; Miao, M.; Lv, J.; Zhu, L.; Liu, H.; Ma, Y. An effective structure prediction method for layered materials based on 2D particle swarm optimization algorithm. *J. Chem. Phys.* **2012**, *137*, 224108. [CrossRef]
22. Lv, J.; Wang, Y.; Zhu, L.; Ma, Y. Particle-swarm structure prediction on clusters. *J. Chem. Phys.* **2012**, *137*, 084104. [CrossRef]
23. Zhang, J.; Lv, J.; Li, H.; Feng, X.; Lu, C.; Redfern, S.A.T.; Liu, H.; Chen, C.; Ma, Y. Rare helium-bearing compound FeO_2He stabilized at deep-earth conditions. *Phys. Rev. Lett.* **2018**, *121*, 255703. [CrossRef]
24. Sun, Y.; Lv, J.; Xie, Y.; Liu, H.; Ma, Y. Route to a superconducting phase above room temperature in electron-doped hydride compounds under high pressure. *Phys. Rev. Lett.* **2019**, *123*, 097001. [CrossRef]
25. Huang, P.; Liu, H.; Lv, J.; Li, Q.; Long, C.; Wang, Y.; Chen, C.; Hemley, R.J.; Ma, Y. Stability of H_3O at extreme conditions and implications for the magnetic fields of Uranus and Neptune. *Proc. Natl. Acad. Sci. USA* **2020**, *117*, 5638. [CrossRef] [PubMed]
26. Zhang, J.; Liu, H.; Ma, Y.; Chen, C. Direct H-He chemical association in superionic FeO_2H_2He at Deep-Earth conditions. *Natl. Sci. Rev.* **2021**. [CrossRef]
27. Yong, X.; Liu, H.; Wu, M.; Yao, Y.; Tse, J.S.; Dia, R.; Yoo, C.S. Crystal structures and dynamical properties of dense CO_2. *Proc. Natl. Acad. Sci. USA* **2016**, *113*, 11110–11115. [CrossRef] [PubMed]
28. Perdew, J.P.; Burke, K.; Ernzerhof, M. Generalized gradient approximation made simple. *Phys. Rev. Lett.* **1996**, *77*, 3865. [CrossRef]
29. Kresse, G.; Furthmuller, J. Efficient iterative schemes for ab initio total-energy calculations using a plane-wave basis set. *Phys. Rev. B Condens. Matter Mater. Phys.* **1996**, *54*, 11169. [CrossRef]
30. Togo, A.; Oba, F.; Tanaka, I. First-principles calculations of the ferroelastic transition between rutile-type and $CaCl_2$-type SiO_2 at high pressures. *Phys. Rev. B Condens. Matter Mater. Phys.* **2008**, *78*, 134106. [CrossRef]
31. Hongzhiwei Technology, Device Studio, Version 2021A, China. 2021. Available online: https://iresearch.net.cn/cloudSoftware (accessed on 7 September 2021).
32. Bader, R. A quantum theory of molecular structure and its applications. *Chem. Rev.* **1991**, *91*, 893. [CrossRef]
33. Baroni, S.; Giannozzi, P.; Testa, A. Green's-function approach to linear response in solids. *Phys. Rev. Lett.* **1987**, *58*, 1861. [CrossRef]
34. Giannozzi, P.; De Gironcoli, S.; Pavone, P.; Baroni, S. Ab initio calculation of phonon dispersions in semiconductors. *Phys. Rev. B* **1991**, *43*, 7231. [CrossRef] [PubMed]
35. Giannozzi, P.J. QUANTUM ESPRESSO: A modular and open-source software project for quantum simulations of material. *Phys. Condens. Matter* **2009**, *21*, 395502. [CrossRef] [PubMed]
36. Giannozzi, P. Advanced capabilities for materials modelling with QUANTUM ESPRESSO. *J. Phys. Condens. Matter* **2017**, *29*, 465901. [CrossRef] [PubMed]

37. Wei, S.; Zhu, C.; Li, Q.; Zhou, Y.; Li, Q.; Ma, Y. High-pressure phase transition of cesium chloride and cesium bromide. *Phys. Chem. Chem. Phys.* **2014**, *16*, 17924. [CrossRef]
38. Allen, P.B. Neutron Spectroscopy of Superconductors. *Phys. Rev. B* **1972**, *6*, 2577. [CrossRef]
39. Allen, P.B.; Dynes, R.C. Transition temperature of strong-coupled superconductors reanalyzed. *Phys. Rev. B* **1975**, *12*, 905. [CrossRef]
40. Dominik, S.; Adam, Z.K.; Ewa, A.D.S.; Radosław, S. Phonon-mediated superconductivity in bismuthates by nonadiabatic pairing. *Phys. Rev. B* **2021**, *104*, 094501.
41. Dominik, S.; Radosław, S. Signatures of nonadiabatic superconductivity in lithium-decorated graphene. *Phys. Rev. B* **2019**, *99*, 224512.